Micromachined Reactors for Catalytic Partial Oxidation Reactions

Ravi Srinivasan, I-Ming Hsing, Peter E. Berger, Klavs F. Jensen
Dept. of Chemical Engineering, Massachusetts Institute of Technology, MIT 66-566, 77 Massachusetts Ave., Cambridge, MA 02139

Samara L. Firebaugh and Martin A. Schmidt
Dept. of Electrical Engineering and Microsystems Technology Laboratory, Massachusetts Institute of Technology, Cambridge, MA 02139

Michael P. Harold, Jan J. Lerou, and James F. Ryley
DuPont Company, Central Research & Development, Experimental Station, Wilmington, DE 19880

Silicon-based microfabrication of a novel chemical reactor (microreactor) having submillimeter flow channels with integrated heaters, and flow and temperature sensors is described. The potential application of this reactor to partial-oxidation reactions is explored by using Pt-catalyzed NH_3 oxidation as a model reaction. Investigation of reactor behavior as a function of operating conditions shows that conversion and selectivity behavior of conventional laboratory reactors can be reproduced and demonstrates the feasibility of conducting chemical reactions in microfabricated systems. Ignition-extinction behavior is explored, along with high-temperature microreactor materials degradation. Potential applications and scale-up of microreactors are also discussed.

Introduction and Motivation

The chemical industry currently operates reactors in a few large facilities to achieve economies of scale. Often chemical intermediates are subsequently shipped to smaller plants, where they are further processed. For example, monomers may be shipped to a small fibers plant where continuous polymerization and polymer processing steps are carried out. Large-scale chemical production and transportation raise environmental and safety concerns. Recent reports have suggested point-of-use, on-demand production in miniaturized chemical systems (minichemical systems) for improved safety by eliminating storage and transportation of toxic and hazardous chemicals and reducing potential damage due to accidents (Benson and Ponton, 1993; Lerou et al., 1996). The emerging technology of micromachining has several advantages for fabricating reactors (microreactors) for these minichemical systems.

Micromachining uses standard integrated-circuits manufacturing steps such as thin-film deposition, ion implantation, lithography, and etching to machine miniature mechanical devices with feature sizes of 1 μm to 100 μm. While this technology is currently used to manufacture sensors and analytical instruments (Wise and Najafi, 1991; Harrison et al., 1993), it also offers the ability to design reactors that are inherently safe for potentially explosive reactions. The safety potential of the microreactors stems from the defined small channels, and the ability to integrate sensors on-chip for early detection of runaway reactions. The small channels of the microreactor and the corresponding large surface area to volume ratios would serve to inhibit gas-phase free-radical reactions, as well as improve heat transfer for exothermic reactions. These features would be particularly advantageous for hydrocarbon partial-oxidation reactions, which comprise fast, short contact time reactions used for producing oxygenates (e.g., aldehydes, alcohols) and nitrogen-bearing compounds (e.g., cyanides, nitriles, and cyanates) for polymers and agricultural products (Satterfield, 1991). Many of the products are toxic, making them ideal candidates for point-of-use production. In addition, the high exothermicity ($\Delta H_{r\times n} \sim -100$ kJ) makes the control of current partial-oxidation reactors, such as fixed-bed and gauze reactors, difficult (Morbidelli and

Correspondence concerning this article should be addressed to K. F. Jensen.

Varma, 1988; Froment and Bischoff, 1990; Schmidt et al., 1994). While the large surface area to volume ratio of microreactors is an advantage for preventing free-radical runaway reactions, it precludes chemical production by rapid quenching of gas-phase chemical intermediates (Goetsch and Schmidt, 1996).

Recently, several groups have demonstrated reactions in externally heated microchannels that were precision machined by conventional technologies (Hönicke and Weissmeier, 1996; Jäckel, 1996; Wegeng et al., 1996), and microfabricated on silicon wafers (Lerou et al., 1996). Integrated chemical devices, such as a reactor–heat-exchanger module (Lerou et al., 1996) and micromixer reaction chamber (Ehrfeld et al., 1996), have also been fabricated.

Integration of additional functions on a microreactor, such as sensors, valves, and heaters, could provide additional safety features. For example, if the sensors detect a potential for thermal runaway, the reactor could be valved off and heaters turned off to prevent the runaway. The ability to integrate sensors and actuators with the reaction channel sets these devices apart from passive small-scale reactors, such as capillary or honeycomb-monolith-based reactors. To test these concepts, we have microfabricated a chemical reactor (microreactor) with integrated heaters, and flow and temperature sensors.

Scale-up of microreactors can be achieved by configuring several microreactors in parallel. This parallel scale-up route, or "scale-out," has certain advantages over conventional scale-up. Conventional scale-up entails going from laboratory scale to a single large reactor unit through a series of costly laboratory experiments, pilot plant stages, and simulations. In contrast, since each microreactor would behave exactly alike, individually and in replicated units, scale-up would be considerably shorter and less expensive, allowing for faster time to market, and flexible operation in the event of sudden changes in product demand. In certain niche markets, these advantages provided by parallel operation of microreactors could potentially override the economies of scale offered by conventional large plants.

Microreactor Prototype Description

We have micromachined a prototype microreactor (Srinivasan et al., 1996) with submillimeter channels having heaters, and flow and temperature sensors integrated on-chip (Figures 1 and 2). The microreactor consists of a T-shaped channel (in top-view) for gas flow etched in a silicon wafer. The channel is capped from the top by a 1-μm-thick silicon nitride membrane and sealed from the bottom with an aluminum plate having three gas inlet-outlet holes. The reactants enter at the two horizontal ends of the T-shaped channel, mix at the entrance, and react in the vertical reaction channel. The products exit at the vertical end of the T.

The top face of the silicon nitride membrane has thin-film Pt lines deposited, which serve as resistive heaters, and flow and temperature sensors. The flow sensor is a thin-film hot-wire anemometer; the temperature sensor is a thin-film resistance temperature device (RTD) (Doebelin, 1990), both relying on the property that the electrical resistance of Pt increases with temperature. The temperature is determined by comparing the measured electrical resistance of the sensor with previously calibrated values of resistance with temperature. At fixed power and increasing flow rates, convective cooling causes a drop in temperature, leading to a decrease

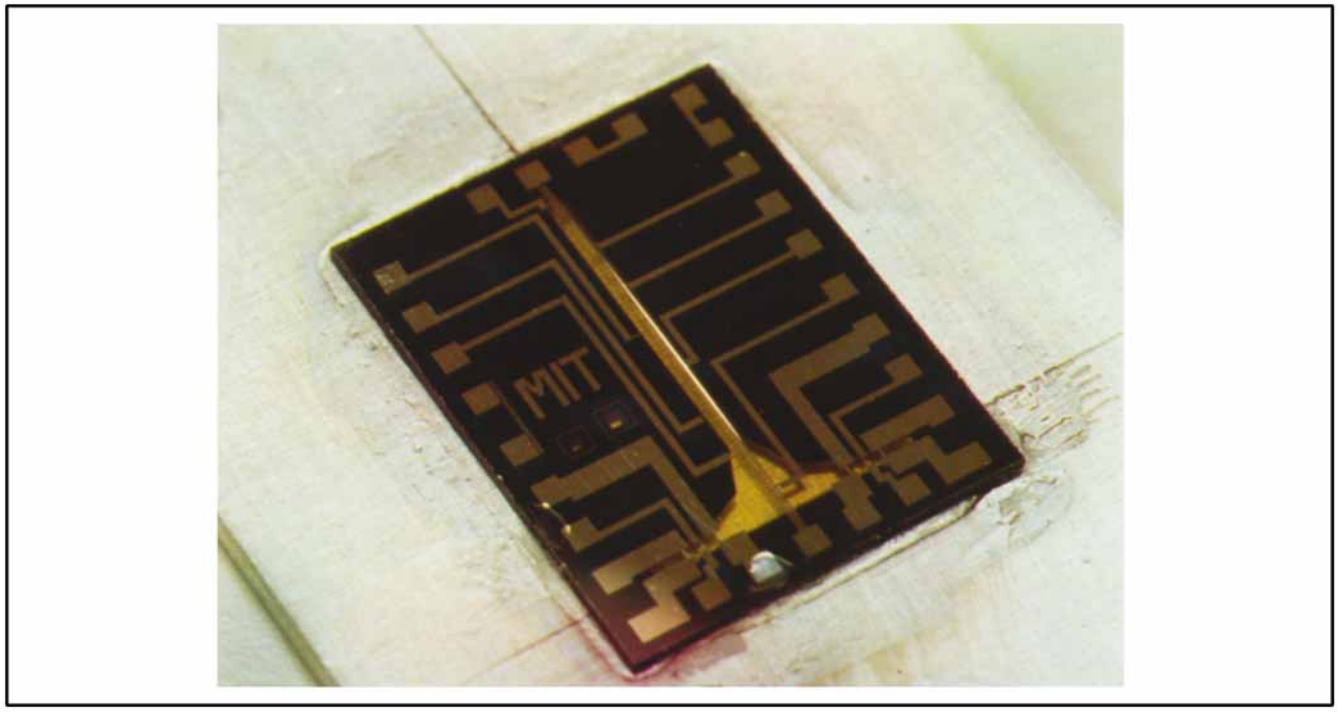

Figure 1. Microreactor showing the Si chip (2.5×1.5 cm^2) epoxied to the Al sealing plate.

Pt metal lines form heaters, flow, and temperature sensors. The lines terminate in bond pads at the edges of the chip (Felice Frankel, MIT).

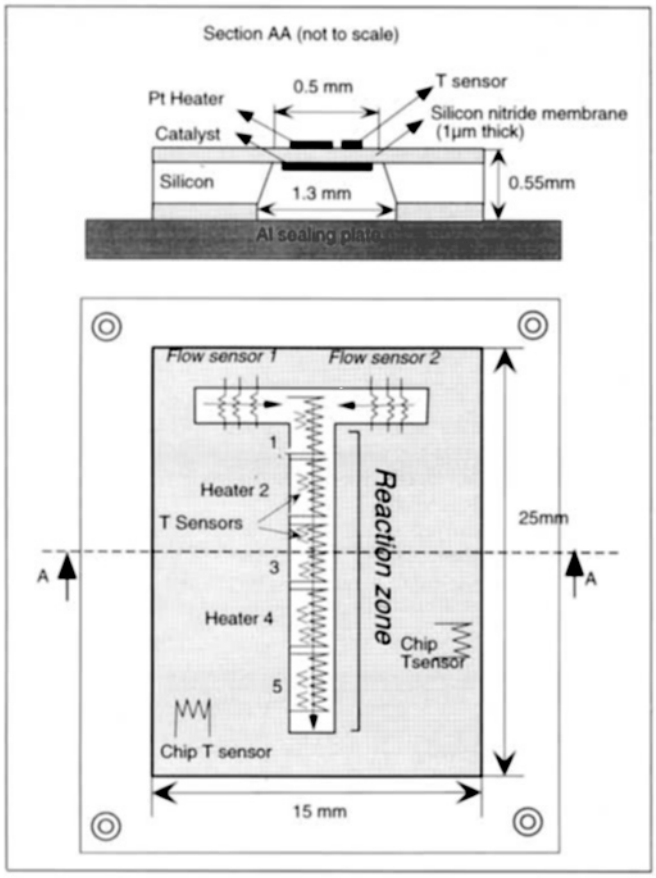

Figure 2. Microreactor showing on-chip components.

The heaters, flow, and temperature sensors are represented as resistors in the top view. The cross-sectional view shows the reaction channel capped from the top by the silicon nitride membrane and sealed from the bottom by the Al sealing plate. The thin-film catalyst, and the heaters and temperature sensors are on opposite faces of the silicon nitride membrane.

in the resistance of the thin-film sensor. By comparing the measured resistance with calibrated values of resistance with flow rates, the actual flow rate can be determined. In the present work, external mass flow controllers were used.

A thin-film Pt catalyst, coated on the bottom face (channel side) of the silicon nitride membrane in the reaction channel, is resistively heated by the thin-film heater deposited on the top face of the membrane, and the temperature is measured by the sensors present adjacent to the heaters (Figure 2). Thus the catalyst is thermally coupled with the heater and temperature sensor by the 1-μm-thick silicon nitride membrane. Simulations show that the temperature variation across the thickness of the silicon nitride membrane is negligible (Hsing et al., 1997), which indicates that the temperature-sensor measurements accurately represent the catalyst temperature.

Fabrication Procedure

The microreactor was fabricated in the clean rooms at MIT's Microsystems Technology Laboratory, using standard micromachining technology (Wise and Najafi, 1991). The starting material for the μ-reactor fabrication (Figure 3) was a double-sided polished (100-mm-dia., 550-μm-thick) silicon

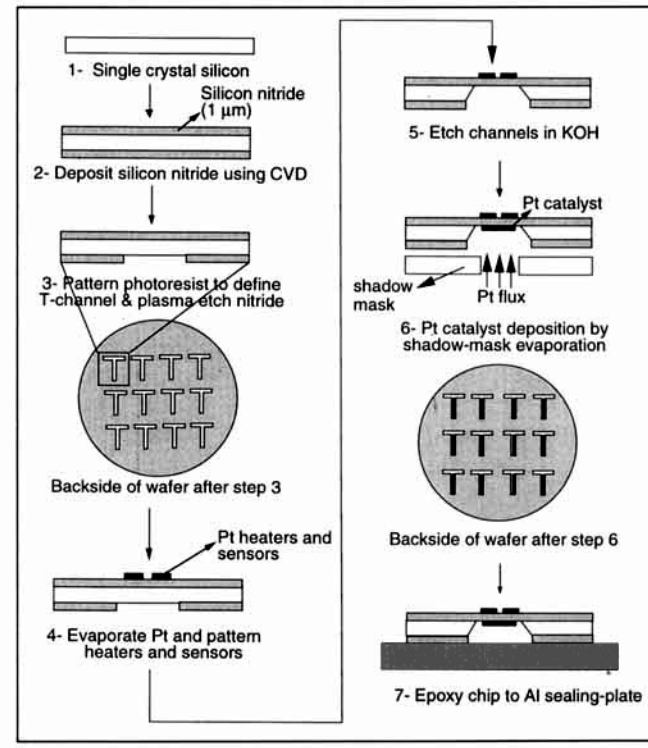

Figure 3. Fabrication process flow for the microreactor.

wafer. The wafer was coated by low-pressure chemical vapor deposition (LPCVD) with 1-μm-thick low-stress silicon nitride (SiN_x) (Sekimoto et al., 1982). The deposit on the frontside of the wafer eventually formed the capping membrane of the microreactor (Figure 2). The SiN_x on the backside of the wafer was patterned using photoresist, and plasma etched (in SF_6) to expose the underlying silicon in the T-shaped channel regions (step 3). The frontside of the wafer was then coated with image-reversal resist for metal deposition, and patterned after alignment to the T-shaped channels on the backside of the wafer (the backside to frontside alignment through the Si wafer was achieved using infrared light). The frontside of the wafer was then coated with 0.1-μm Pt (with 10-nm Ti as an adhesion layer) by electron-beam evaporation, and patterned using metal lift-off to form the metal heaters, and temperature and flow sensors (step 4). The gas flow channels were formed by etching the bulk of the silicon (exposed on the backside of the wafer) in KOH solution (20% by weight in water at 90°C). KOH anisotropically etches Si along $\langle 111 \rangle$ planes, thus forming channels that are trapezoidal in cross section (Figures 2 and 3). Since SiN_x is not attacked by KOH, the etch terminates on the SiN on the frontside of the wafer, thus forming the SiN_x capping membrane (step 5). A custom-built sealing plate was used to protect the Pt on the frontside of the wafer from KOH during this etch. Subsequently, a 0.1-μm-thick platinum catalyst (on 10-nm Ti) film was selectively deposited on the silicon nitride membrane in the reaction channel by electron-beam evaporation via a shadow mask (step 6). The wafer was then diced into 12 individual chips, and each chip was epoxied to an aluminum base-plate with three gas inlet–outlet holes (step 7).

Test Setup

The microreactor was mounted on a custom-built gas-feedthrough Al block (Figure 4). The two inlets and the outlet of the microreactor were aligned to the corresponding holes in the block, and compression sealed using O-rings. The gas inlet and outlet holes in the block were connected to external 1/16-in.-dia. (1.6-mm-dia.) stainless-steel pipes that were Swagelock fitted to the block. Gaseous reactants from cylinders were fed by external mass-flow controllers that maintained the desired flow rates. The microreactor exhaust composition was continuously monitored using a quadrupole mass spectrometer. Because of the small volumetric throughput of the microreactor (~ 10 std. cm^3), care was taken to minimize any dead volumes between the microreactor and the mass spectrometer to prevent signal delays and signal convolutions due to gas mixing. Since conventional leak valves have large dead volumes, a 3.8-cm-long, 15-μm-ID fused-silica capillary tube was used to introduce gases from the exhaust tubing (760 torr) into the mass-spectrometer chamber (which was maintained at 1×10^{-5} torr).

Electrical connections to the on-chip bond pads of the heaters and sensors were made using a probe card. The microreactor bond pads were aligned and contacted to the tungsten probes of the probe card using an x-y-z-stage and a microscope. The probe card was plugged into an edge connector for power supply and sensor readout. The power supply to the on-chip heaters was operated in a constant-current mode and the current, and voltage readings were collected on a PC-based data-acquisition system. The measured electrical resistance was also logged into the PC and converted into temperature readings using a previously generated calibration curve. The electrical resistance-temperature behavior of thin-film Pt was studied and calibrated using a custom-built test setup that allowed measurements up to 1,100°C. The electrical resistance of 0.1-μm-thick Pt (on 10-nm Ti adhesion layer) increased linearly with temperatures up to 800°C, consistent with observations with bulk Pt films (Omega, 1992). Above 800°C, however, the electrical resistance increased exponentially, due to material degradation. This places the upper limit on temperature measurements at 800°C.

The electrical resistance was expressed as

$$R = R_o \times [1 + \alpha(T - T_o)], \tag{1}$$

where R is the resistance at temperature T, R_o is the resistance at a reference temperature T_o, and α is the temperature coefficient of resistance 2.86×10^{-3}/°C. This value is slightly lower than the value for bulk Pt 3.85×10^{-3}/°C (Omega, 1992).

Results and Discussion

Temperature profiles in inert-gas environment

Experiments and simulations were carried out to determine the temperature profiles in the microreactor in inert-gas flow. At a given flow rate of inert gas (O_2), power was supplied to the heater segment 4 (Figure 2), and the temperature monitored using the on-chip temperature sensors adjacent to the heater segment (see, e.g., Figure 5). Each temperature sensor was geometrically identical and provided spatially averaged (650-μm$\times$250-μm) temperature measurements. Experiments showed that the temperature profile was uniform to within 10% along the axis of the heater (Figure 6), with a sharp falloff outside the heater segment. The temperature drops to less than 10% of the maximum at an axial distance of 700 μm from the edge of the heater segment, and to room temperature 1,700 μm from the heater edge. The sharp axial falloff in temperature has been verified by three-dimensional finite-element simulations (Figure 7) (Hsing et al., 1997). Since the characteristic dimension of the microreactor was 0.5 mm and the microreactor was operated at atmospheric pressures, the Knudsen number is sufficiently small ($Kn \sim 10^{-4}$) that continuum transport analysis applied to the cases considered in this work. Simulations further revealed

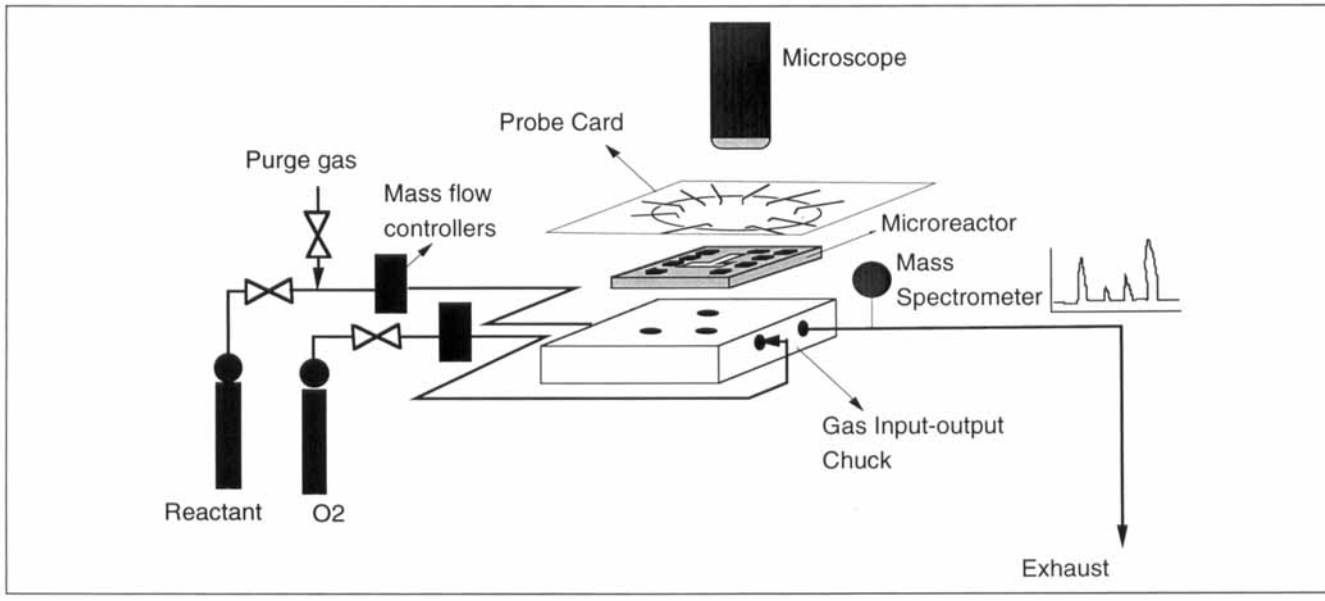

Figure 4. Test setup for the microreactor.

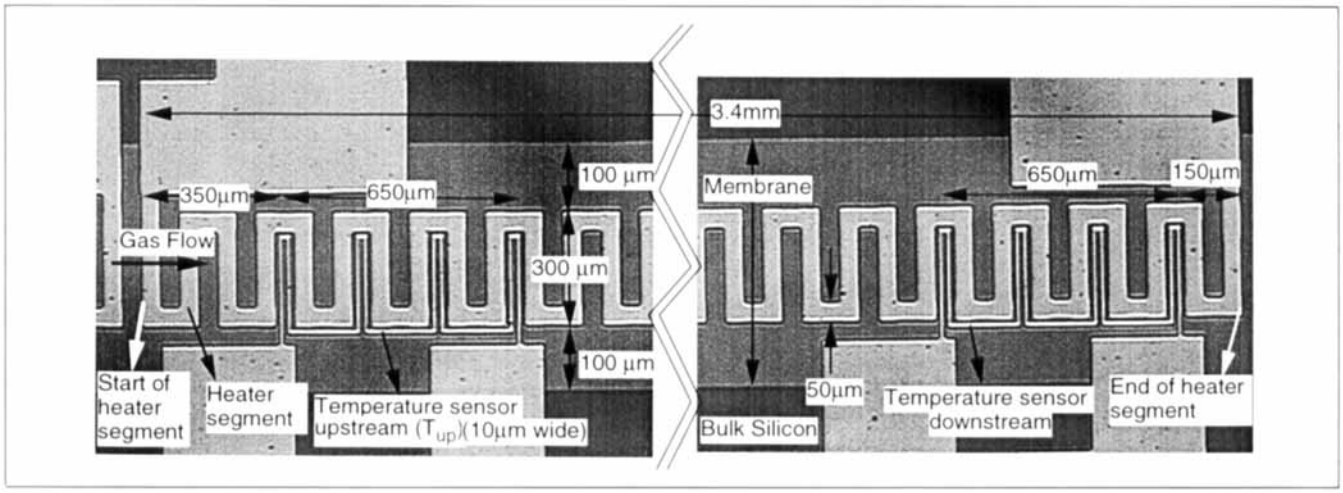

Figure 5. Image of one of the heater segments (#3) showing the position of temperature sensors and the relevant dimensions.

that the hot zone was localized to the membrane and adjacent gas, while the channel walls were at room temperature (Figure 7a). The excellent thermal conductivity of the bulk silicon (141 $W/m^2/°C$) and its large thickness (550 μm) relative to the SiN_x membrane (1 μm), contribute to preventing chain-branching runaway reactions. Simulations also showed convection effects in the microreactor with increasing gas flow rates (Figure 7b). The upstream temperature dropped significantly at larger flow rates, while the downstream temperature remained constant. The simulations are in excellent agreement with experimental results (Figure 7c).

Ammonia oxidation in microreactor

Ammonia oxidation was chosen as the candidate reaction for microreactor studies because it is well understood (Pignet and Schmidt, 1974; Bradley et al., 1995), highly exothermic,

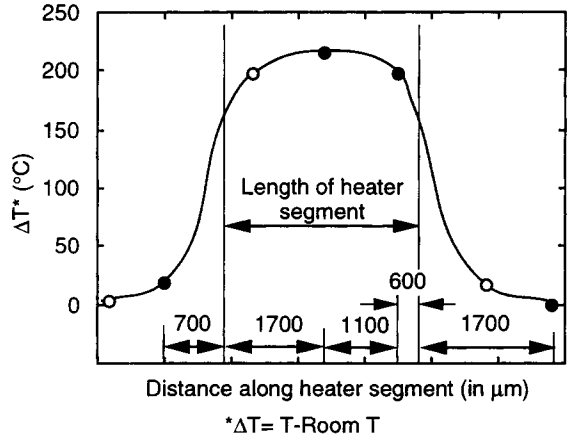

Figure 6. Axial temperature profile in heater segment 4 in inert ambient and under no-flow conditions.

The hot zone is localized to the heater segment, while the temperature falls off rapidly outside the heater segment. The solid points represent the placement of actual temperature sensors, and the open points are obtained from symmetry considerations of the temperature profile under no-flow conditions.

without catalyst contamination by carbon, and has several series and parallel reaction pathways allowing for selectivity studies. The desired product of the reaction is NO, while N_2 production represents product loss. Ammonia oxidation is used industrially in the production of nitric acid, and constitutes an important step in ammoxidation reactions used to produce nitrogen-bearing compounds for agricultural chemicals and monomers (Satterfield, 1991). The major overall reactions in previously proposed mechanisms (Pignet and Schmidt, 1974; Pignet and Schmidt, 1975) are

$$NH_3 + \frac{5}{4}O_2 \xrightarrow{Pt} NO + \frac{3}{2}H_2O + 226\ kJ \qquad (R1)$$

$$NH_3 + \frac{3}{2}NO \xrightarrow{Pt} \frac{5}{4}N_2 + \frac{3}{2}H_2O + 454\ kJ \qquad (R2)$$

$$2NO \xrightarrow{Pt} N_2 + O_2 + 90\ kJ \qquad (R3)$$

$$NH_3 \xrightarrow{Pt} \frac{1}{2}N_2 + \frac{3}{2}H_2 - 47\ kJ \qquad (R4)$$

$$H_2 + \frac{1}{2}O_2 \xrightarrow{Pt} H_2O + 242\ kJ. \qquad (R5)$$

Reaction experiments were conducted on heater segment 3 (Figures 2 and 5), which was 3.4 mm long and had two temperature sensors—an upstream temperature sensor 350 μm from the beginning of the heater segment, and a downstream temperature sensor 150 μm from the end of the heater segment. In a typical experimental run, the power supplied to the heater was increased at a fixed inlet composition and flow rate of NH_3 and O_2. Ignition occurred at $\sim$200°C in the center of the heater segment, resulting in a temperature rise due to heat of reaction (Figure 8). At operating flow rates ($<$15 std. cm^3/min), the ignition front quickly traveled upstream and stabilized at the entrance region of the heater, resulting in higher temperature upstream, while the downstream temperature remained at $\sim$200°C. Upon ignition, the NH_3 peak dropped in the mass-spectrometer output of the

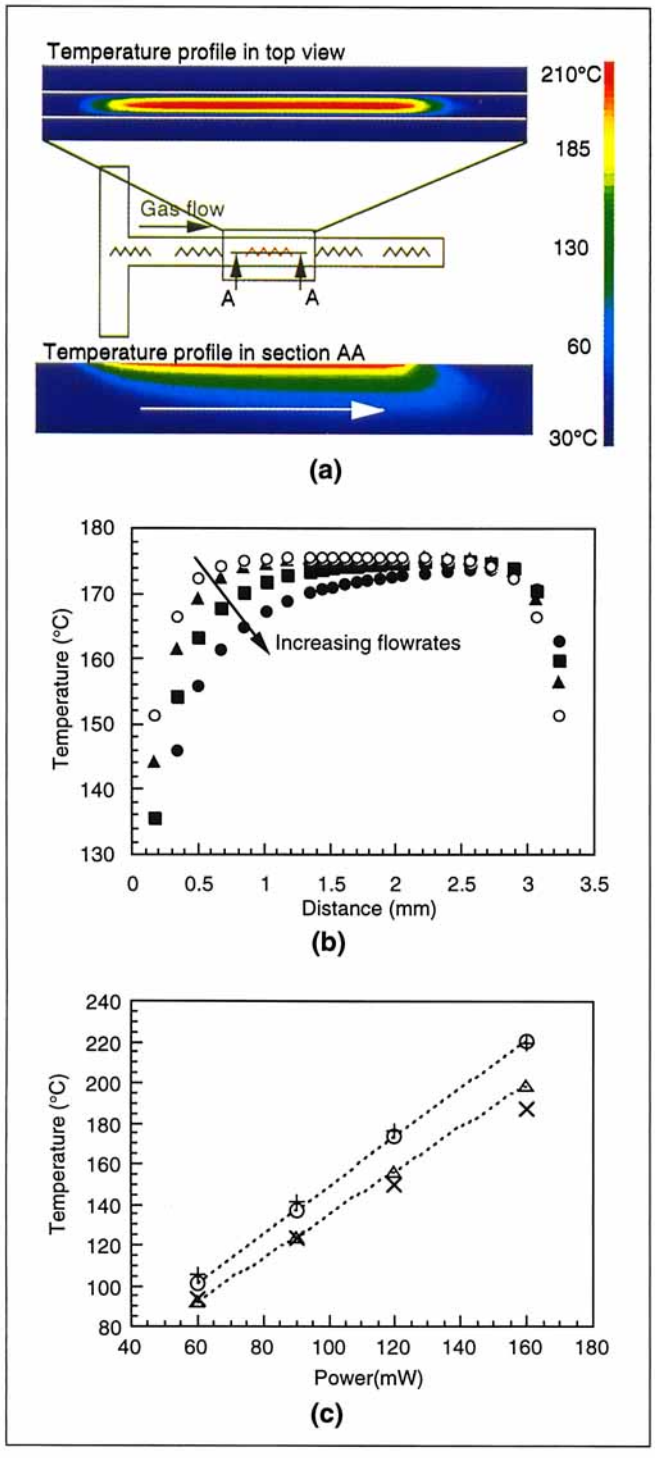

Figure 7. (a) Simulation of temperature profiles in a single heater segment of the microreactor under 20 std. cm³/min flow of O_2; (b) simulation of axial temperatures in the microreactor showing heat convection at increasing flow rates of O_2; (c) comparison of simulations with experimental data.

The hot zone is localized to the SiN membrane and adjacent gas, while the edges of the membrane and the bulk Si are at room temperature. ○: 0 std/ cm³/min; ▲: 10 std. cm³/min; ■ 25 std. cm³/min; ●: 50 std. cm³/min flow. △, downstream; ○ upstream circles; ×, downstream; +, upstream temperatures.

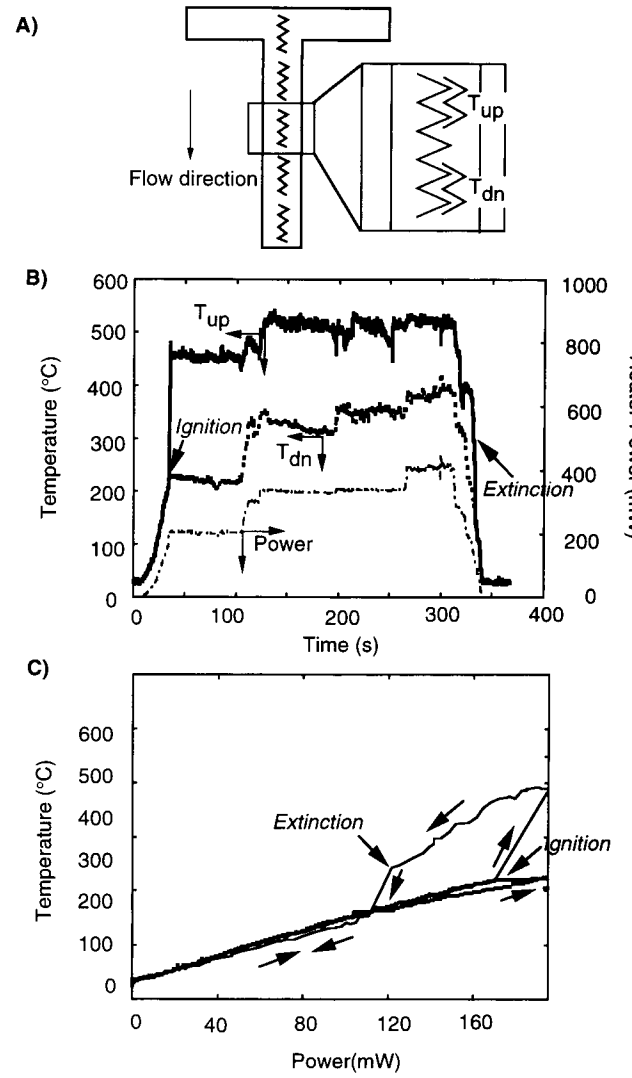

Figure 8. (a) Microreactor showing active heater segment and position of temperature of sensors; (b) typical experimental result showing measured temperatures and heater powers with time; (c) temperature–power diagram showing hysteresis behavior on the upstream temperature sensor, while the downstream sections did not ignite.

Ignition occurred at 215°C, resulting in temperature rise upstream (T_{up}), while the downstream temperature remained constant (T_{dn}). On decreasing the power, extinction occurred at 300°C. These results were collected at 15% inlet composition of NH_3 in O_2, pressure of 1 atm, and total flow rate of 5 std. cm³/min.

exhaust stream, while the NO and N_2 peaks increased as they were produced (Figure 9). When the heater power was lowered, the ignited area gradually decreased, the downstream sections extinguishing first, and the upstream section eventually extinguishing at temperatures ~ 300°C.

Simulations of the underlying physical chemical phenomena have confirmed that the upstream movement is a result of axial heat conduction in the membrane and the presence of fresh reactants upstream (Hsing et al., 1997). The upstream movement of ignition wave, and the resulting differ-

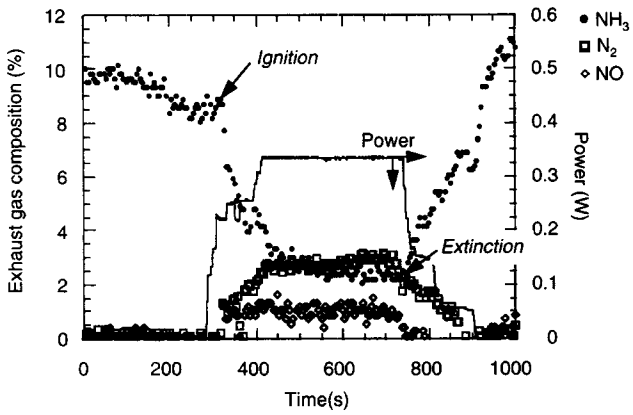

Figure 9. Typical exhaust composition of the microreactor as a function of power.

The NO concentration rises at the expense of N_2 when the heater power and, implicitly, the temperature is increased.

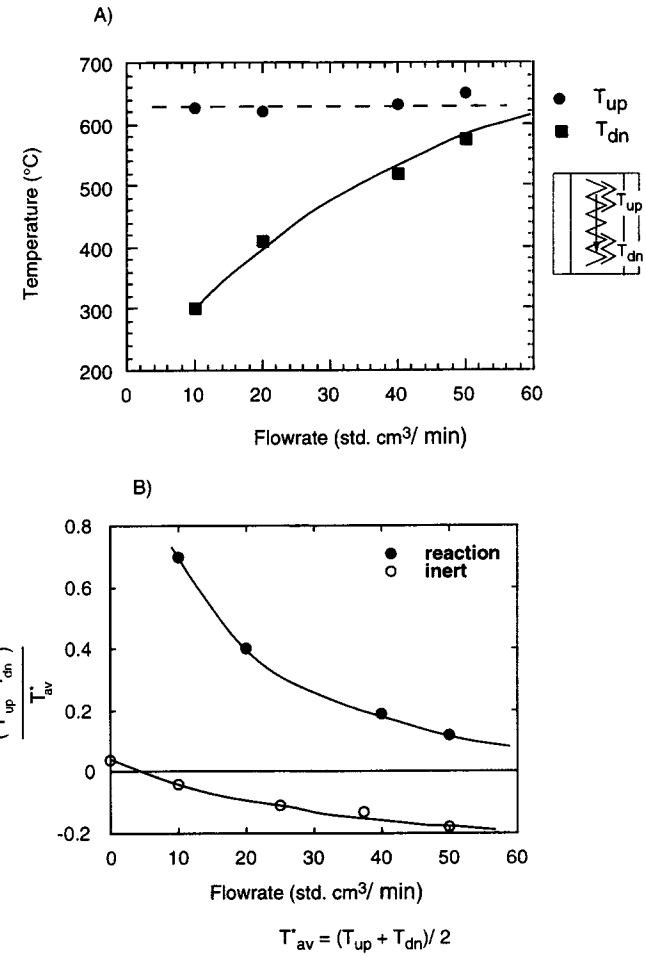

Figure 10. (a) Upstream and downstream temperatures as a function of flow rates for inlet compositions of 10% NH_3 in O_2, and power of 245 ± 25 mW; (b) temperature difference between upstream and downstream sections of the heater segment at varying flow rates.

Convection effects equalize the temperatures along the heater segment at higher flow rates. In inert flow, heat convection results in higher downstream temperatures, while in reactive flow, the opposing effects of upstream heat movement caused by reaction, and downstream convection of reactant and heat can be seen. The temperature difference is not zero at no-flow because of a small asymmetry in placement of sensors (cf. Figure 5).

ence between the upstream and downstream temperatures, was found to vary both with flow rate and inlet composition. At low flow rates, most of the reaction occurred at the entrance region of the heater segment, which consumed a large fraction of the reactants. This reactant depletion resulted in decreased downstream reaction and corresponding low heat-generation rates, and the temperature downstream remained at the ignition value of 200°C. At larger flow rates, however, a significant reaction takes place downstream. This behavior, combined with increased convection, resulted in higher downstream and lower upstream temperatures at large flow rates (Figure 10a).

Figure 10b provides further insight into the relative importance of upstream reaction, and convection on the temperature profiles in the microreactor. In an inert gas flow, the temperature is higher downstream than upstream, even at low flow rates (5 std. cm^3/min), because of convection. In contrast, when a reacting mixture is flowing, both the upstream reaction, as well as the convection of heat and reactants, determine the temperature profile. At low flow rates the temperature upstream is higher, but at large flow rates (> 50 std. cm^3/min), convection effects equalize the temperature profile along the heater segment.

The ignition temperature (~ 200°C) was found to be independent of the inlet composition. However, the temperature rise after ignition in the upstream temperature sensor increased at inlet compositions that were close to stoichiometry (Figure 11), which is consistent with observations in conventional laboratory reactors (Williams et al., 1991). Experiments closer to stoichiometric mixtures were not conducted since the microreactor membrane degraded and ruptured at temperatures higher than ~ 650°C.

The temperature rise after ignition, and the corresponding thermal expansion, deformed the microreactor membrane (Figure 12), with increased deformations at larger temperatures. The deformations were visible at temperatures higher than 300°C. Although the deformation is undesirable from the standpoint of mechanical integrity of the membrane, it was a convenient research feature, allowing visualization of the progress of reaction (Figure 12). Video images of the membrane buckling showed that the ignition front moved upstream within 66 ms after igniting, reaching steady state after 160 ms.

Conversion and selectivity were explored as a function of heater power, flow rate (contact time), and inlet composition. The primary products of the reaction were NO and N_2 (Figure 9). N_2O was formed in small quantities (< 15%) at temperatures below 350°C and was absent at temperatures higher than 400°C due to N_2O decomposition, consistent with conventional reactor studies (Pignet and Schmidt, 1974). The selectivity ratio of NO to N_2 increased dramatically with heater power (Figures 9 and 13). The strong selectivity increase with temperature is also consistent with conventional laboratory reactor data (Pignet and Schmidt, 1974), and is likely caused by a low NO residence time on the catalyst sur-

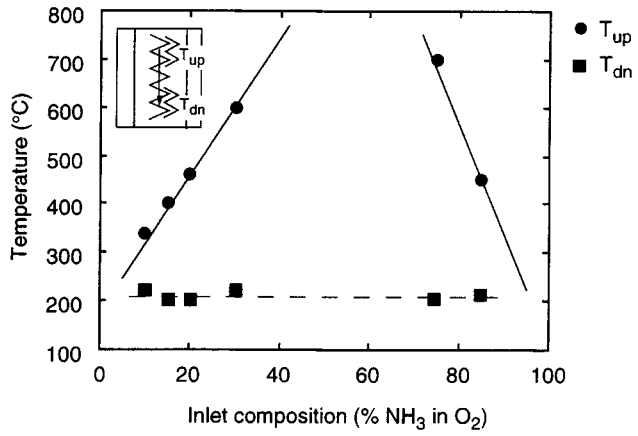

Figure 11. Upstream and downstream temperatures with changing inlet composition of NH_3 in O_2.

All data were collected at a total flow rate of 5 std. cm^3/min, pressure of 1 atm, and heater power of 188 ± 12 mW.

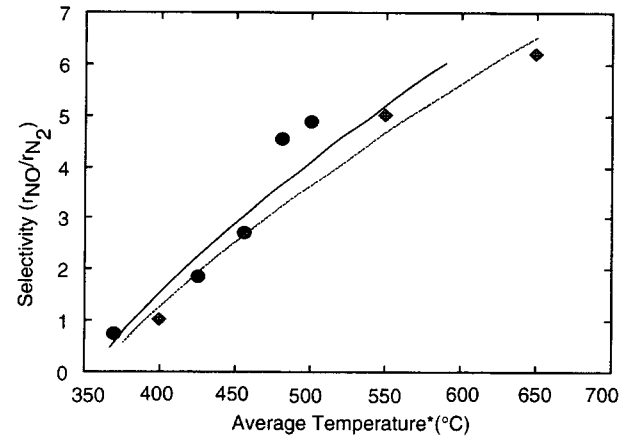

Figure 13. Selectivity variation with temperature for the microreactor and comparison with conventional laboratory reactors.

●, microreactor data 10% NH_3 in O_2; ◆, conventional laboratory reactor, 5.3% NH_3 in air, 20% NH_3 in O_2.

face, preventing NO dissociation (reaction 3) (Bradley et al., 1995) and reaction with NH_3 (reaction 2) (Pignet and Schmidt, 1974).

After ignition, as the heater power was further increased, the conversion increased slightly with the spreading of the reaction to downstream sections of the heater. However, increases in conversion with heater power were much less than could be expected from a simple consideration of reaction-rate increase with temperature, indicating that the reaction was mass-transfer limited after ignition. The maximum conversion obtainable increased with contact-time, with complete conversion observed at contact-time > 9 ms (Figure 14).

This conversion–contact-time behavior indicates that the reaction becomes residence-time limited with significant fractions of the reactants bypassing the catalyst at higher flow rates. The selectivity of NO to N_2 decreases with contact time since larger contact times allow NO to readsorb and further dissociate (reaction 3) (Bradley et al., 1995) and/or react with NH_3 (reaction 2) (Pignet and Schmidt, 1974) to produce N_2. Thus a classic conversion-selectivity trade-off is observed with contact time. The conversion was found to be independent of inlet composition. However, the selectivity dropped to 0% when operating in NH_3-rich conditions because NH_3 inhibits NO desorption (Pignet and Schmidt, 1974).

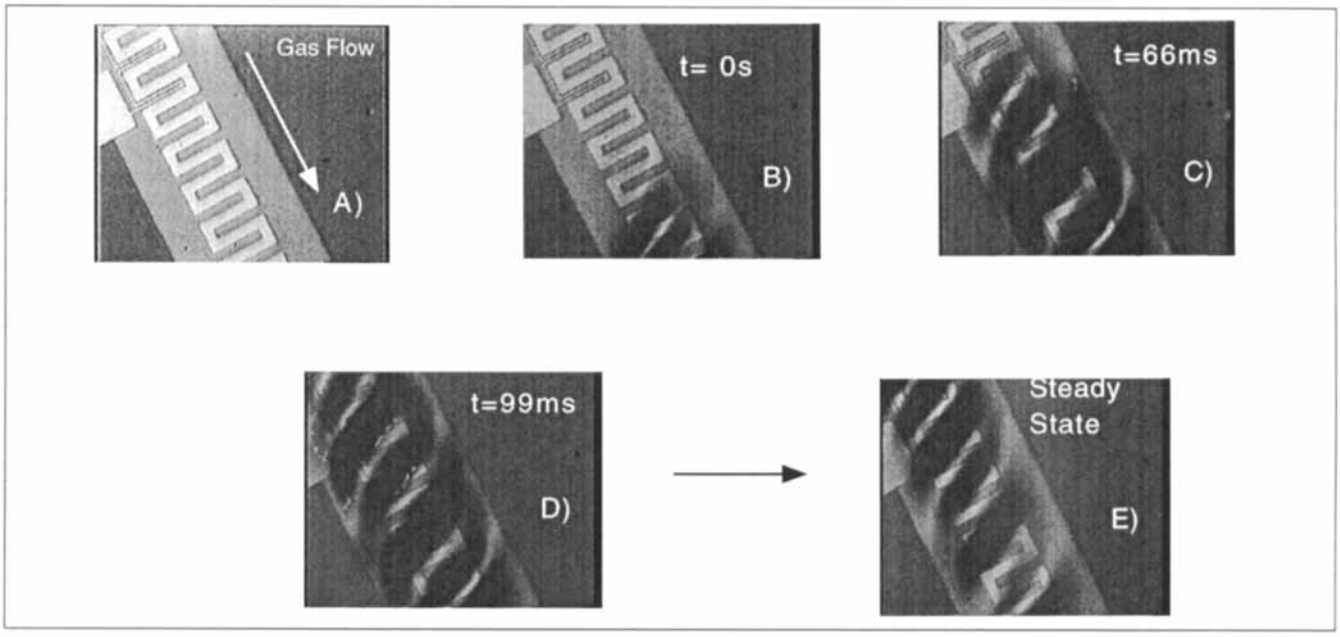

Figure 12. Video frames of membrane deformation due to temperature rise and upstream movement of an ignition front in the microreactor.

The ignition front eventually stabilizes in the entrance region of the heater.

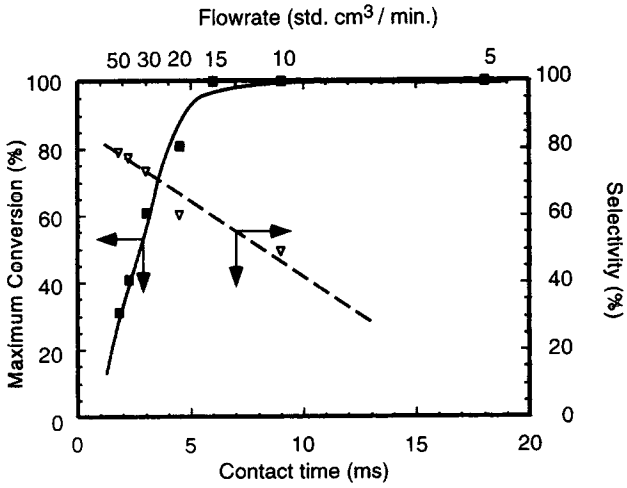

Figure 14. Maximum conversion and selectivity in a single heater segment of microreactor as a function of contact time (flow rate).

All data were collected at an inlet NH_3 to O_2 ratio of 10% and average catalyst temperature of 425° ± 25°C.

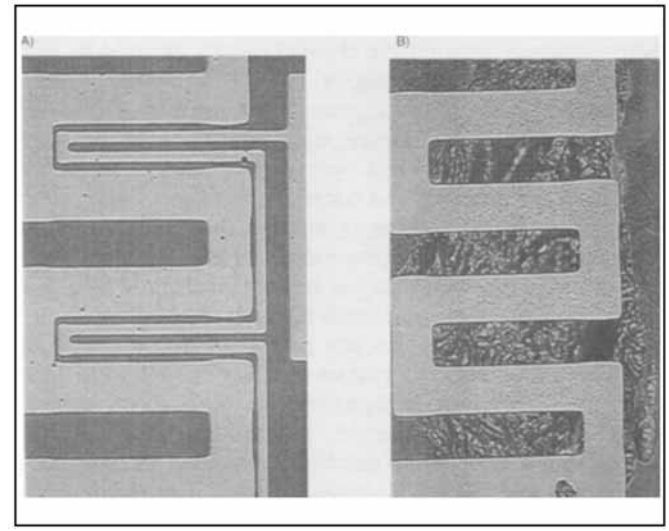

Figure 15. (a) Fresh microreactor; (b) degraded microreactor.

The Pt catalyst has been etched and the heater material has visibly degraded, with pinhole formation after operation at 600°C for ~ 0.5 h.

The ammonia oxidation test results suggest design changes for improving conversion and selectivity in microreactors. In the current design, at low flow rates, most of the reaction occurs in a small upstream section of the heater segment (~ 1 mm), while a large section downstream (2.4 mm) is unutilized. Therefore, shorter heater segments would allow more efficient use of microreactor area. It is also observed that large contact-times are needed for complete conversion, since the reaction is limited by reactant diffusion to the catalyst surface. However, the selectivity drops at large contact times. Building a microreactor that has catalyst on both the top and bottom face of the channel would reduce the diffusion time, and large conversions can then be obtained at low contact times, while maintaining high selectivities.

Microreactor materials stability issues

We have observed microreactor degradation when operating at elevated temperatures. Large mechanical stresses in the SiN membrane, caused by thermal expansion, deform and eventually rupture the membrane at temperatures > 700°C. Membrane stability was improved by increasing the thickness, and alternative materials systems and designs are being explored to further improve the stability. Visual observation of the reactors after operation also indicated that thin-film Pt heaters and the temperature sensors began to degrade at temperatures > 700°C (Figure 15). However, *in-situ* experiments revealed that the electrical characteristics of the heaters and temperature sensors were consistent and repeatable during short-term operation up to 800°C.

At temperatures < 700°C, the microreactor lifetime was limited by the Pt catalyst etching by the reactant mixture of NH_3 and O_2 (Figure 15). We operated the microreactor for ~ 1 h at 600°C before the 0.1-μm-thick Pt catalyst is etched. The etching behavior is also observed in conventional reactors (Satterfield, 1991). While there is agreement in the literature that Pt is lost to the gas stream, there is disagreement regarding the specific mechanism by which catalyst is lost. Flytzani-Stephanopoulos and Schmidt proposed formation of volatile PtO_2, at temperatures ~ 800°C, as the etching mechanism (Flytzani-Stephanopoulos et al., 1977; Flytzani-Stephanopoulos and Schmidt, 1979). It has also been proposed that the Pt reacts with gas-phase radicals, for example, HO_2, to form volatile metastable complexes that are lost to the gas-phase (Dean et al., 1988; Hess and Phillips, 1992). Lyubovsky and Barelko (1994) proposed that the pure Pt from the grain boundaries sublimates due to the coupled effects of enhanced catalytic activity, causing increased temperature and the weak binding of Pt atoms at grain boundaries. The low operating temperatures (400°C–600°C) in the microreactor suggests that PtO_2 formation, as an etching mechanism, is unlikely. Further, etching is not observed in the Pt heater and sensors, which are exposed to air and are at the same temperature at the Pt catalyst, indicating that both NH_3 and O_2 have a role to play in the catalyst etching in the microreactor.

Microreactor Scale-Up for Point-of-Use Production

Microreactors could be used for point-of-use manufacture of chemicals that are required in small quantities. The productivity of the microreactor calculated using the conversion and selectivity data (Figure 14) is 0.6 mol NO produced/s/m^2 of Pt catalyst. Based on this productivity and catalyst area of the prototype microreactor, ~ 10 kg/d of NO (3.65 ton/yr) can be produced by operating 1,000 prototype microreactors in parallel. The throughput can be increased both by increasing productivity, for example, by operating at higher temperatures for increased selectivity in the case of NH_3 oxidation, and by increasing the catalyst area in the microreactor. The increase in catalyst area can be achieved by covering a larger area of the channel (the walls and the floor) by catalyst, and increasing the number of channels per microreactor. The microreactor photograph (Figure 1) shows that large areas of the microreactor is unused for reaction. The reaction channel

density could be increased in future microreactor designs, with the upper limit on the channel density dictated by heat transfer out of the microreactor.

Developing an efficient packaging scheme that provides fluid transport and electrical interconnections to the many thousands of microreactors operating in parallel, is critical for successful scale-up and commercialization of microreactors. One possible packaging scheme, borrowed from the electronics industry, is to plug individual microreactors into a "mixed circuit board" that has flow channels, and also provides electrical interconnections (Berg et al., 1996).

The smaller throughputs and potentially higher packaging costs indicate that microreactors would be used in niche markets where they provide significant advantages over conventional reactors, for example, point-of-use production of toxic/hazardous materials and chemicals requiring faster time to develop and market. The small channel size also requires the use of filters to avoid plugging of channels by particles. While further research is required to address scale-up issues, the current design and operation of a single microreactor could be used as a laboratory platform for kinetic studies. The advantages provided by microreactors for kinetic studies include safety, low reactant usage, less waste, and well-defined geometries that allow relatively simple simulations for better understanding of reaction kinetics. We have ignited highly flammable mixtures without diluents (e.g., 20% H_2 and O_2, NH_3 and O_2 at all compositions, C_2H_6 and O_2 at all compositions) in the microreactor, without an explosion. In some cases, the high-temperature-induced differential thermal expansion ruptured the membrane, releasing the reactants into air, but the small volumes were quickly diluted in the exhaust system.

Conclusions

Microfabrication technology allows fabrication of novel chemical reactors that could have several advantages over conventional techniques. Micromachined chemical reactor systems offer distributed point-of-use chemical manufacturing for safer operation without storage and transportation hazards; ability to tailor reactor geometries of submillimeter to micron dimensions for improved performance; improved process control by integrated sensors and actuators; and shorter development time from laboratory to chemical production. To test these concepts, a prototype microreactor having submillimeter channels with integrated heaters, flow and temperature sensors were microfabricated in silicon. Experiments and simulations indicate that one of the unique features of the microreactor is the localized reaction hot zone, while the channel walls and the bulk of the chip are at room temperature. This could potentially make microreactors safer to operate than conventional reactors by suppressing flame formation by quenching gas-phase radicals on the cold reactor walls. The microreactor has been tested using Pt catalyzed NH_3 oxidation as a model reaction. Test results show that conversion and selectivity behavior of conventional reactors can be reproduced, demonstrating feasibility of conducting chemical reactions in microfabricated systems. Scale-up for industrial use could be achieved by operating many microreactors, in parallel, as minichemical systems. The microreactor could also be used for laboratory kinetics studies if run under conditions where chemical kinetics determine reaction rates. Although Si technology was used for the present example because of the established microfabrication technology, other materials such as glass and ceramics may also be used. Additional studies of gas- and liquid-phase reaction systems are needed to evaluate the potential applications of microfabricated chemical systems.

Acknowledgments

The authors thank DuPont and NSF-PYI (Martin Schmidt) for financial support. Partial support from the DARPA Micro Flumes Program (F30602-97-2-0100) is also acknowledged. We also thank DuPont staff and Microsystem Technology Laboratory (MTL-MIT) staff and students for their help.

Literature Cited

Benson, R. S., and J. W. Ponton, "Process Miniaturization—A Route to Total Environmental Acceptability?," *Trans. Chem. Eng.*, **71A**, 160 (1993).

Berg, A. V. D., T. S. J. Lammerink, V. Spiering, and W. Olthuis, "Modular Concept for Miniature Chemical Systems," *Microsystem Technology for Chemical and Biological Microreactors*, Mainz, Germany, DECHEMA, **132**, 109 (1996).

Bradley, J. M., A. Hopkinson, and D. A. King, "Control of Biphasic Surface Reaction by Oxygen Coverage: The Catalytic Oxidation of Ammonia of Pt(100)," *J. Phys. Chem.*, **99**, 17032 (1995).

Dean, V. W., M. Frenklach, and J. Phillips, "Catalytic Etching of Platinum Foils and Thin Films in Hydrogen-Oxygen Mixtures," *J. Phys. Chem.*, **92**, 5731 (1988).

Doebelin, E. O., *Measurement Systems: Application and Design*, McGraw-Hill, New York (1990).

Ehrfeld, W., V. Hessel, H. Möbius, T. Richter, and K. Russow, "Potentials and Realization of Microreactors," *Microsystem Technology for Chemical and Biological Microreactors*, Mainz, Germany, DECHEMA, **132**, 1 (1996).

Flytzani-Stephanopoulos, M., and L. D. Schmidt, "Evaporation Rates and Surface Profiles on Heterogeneous Surfaces with Mass Transfer and Surface Reaction," *Chem. Eng. Sci.*, **34**, 365 (1979).

Flytzani-Stephanopoulos, M., S. Wong, and L. D. Schmidt, "Surface Morphology of Platinum Catalysts," *J. Catalysis*, **49**, 51 (1977).

Froment, G. F., and K. B. Bischoff, *Chemical Reactor Analysis and Design*, Wiley, New York (1990).

Goetsch, D. A., and L. D. Schmidt, "Microsecond Catalytic Partial Oxidation of Alkanes," *Science*, **271**, 1560 (1996).

Harrison, D. J., K. Fluri, K. Seiler, Z. Fan, C. S. Effenhauser, and A. Manz, "Micromachining a Miniaturized Capillary Electrophoresis Based Chemical Analysis System on a Chip," *Science*, **261**, 895 (1993).

Hess, J. M., and J. Phillips, "Catalytic Etching of Pt/Rh Gauzes," *J. Catalysis*, **136**, 149 (1992).

Hönicke, D., and G. Weissmeier, "Heterogeneously Catalyzed Reactions in a Microreactor," *Microsystem Technology for Chemical and Biological Microreactors*, Mainz, Germany, DECHEMA, **132**, 93 (1996).

Hsing, I.-M., R. Srinivasan, M. P. Harold, K. F. Jensen and M. A. Schmidt, "Finite Element Simulation Strategies for Microfluidic Devices with Chemical Reactions," *Tech. Digest, Int. Conf. on Solid State Sensors and Actuators, IEEE*, p. 1015 (1997).

Jäckel, K.-P., "Microtechnology: Application Opportunities in the Chemical Industry," *Microsystem Technology for Chemical and Biological Microreactors*, Mainz, Germany, DECHEMA, **132**, 29 (1996).

Lerou, J. J., M. P. Harold, J. Ryley, J. Ashmead, T. C. O'Brien, M. Johnson, J. Perrotto, C. T. Blaisdell, T. A. Rensi, and J. Nyquist, "Microfabricated Minichemical Systems: Technical Feasibility," *Microsystem Technology for Chemical and Biological Microreactors*, Mainz, Germany, DECHEMA, **132**, 51 (1996).

Lyubovsky, M. R., and V. V. Barelko, "Formation of Metal Wool Structures and Dynamics of Catalytic Etching of Platinum Surfaces during Ammonia Oxidation," *J. Catalysis*, **149**, 23 (1994).

Morbidelli, M., and A. Varma, "A Generalized Criterion for Parametric Sensitivity: Application to Thermal Explosion Theory," *Chem. Eng. Sci.*, **43**, 91 (1988).

Omega Engineering Inc., *The Temperature Handbook*, Vol. 28, Stamford, CT (1992).
Pignet, T., and L. D. Schmidt, "Selectivity of Ammonia Oxidation on Pt," *Chem. Eng. Sci.*, **29**, 1123 (1974).
Pignet, T., and L. D. Schmidt, "Kinetics of Ammonia Oxidation on Pt, Rh, and Pd," *J. Catalysis*, **40**, 212 (1975).
Satterfield, C. N., *Heterogeneous Catalysis in Industrial Practice*, McGraw-Hill, New York (1991).
Schmidt, L. D., M. Huff, and S. S. Bharadwaj, "Catalytic Partial Oxidation Reactions and Reactors," *Chem. Eng. Sci.*, **49**, 3981 (1994).
Sekimoto, M., H. Yoshihara, and T. Ohkubo, "Silicon Nitride Single-Layer X-Ray Mask," *J. Vac. Sci. Technol.*, **21**, 1017 (1982).
Srinivasan, R., I. M. Hsing, M. P. Harold, J. F. Ryley, K. F. Jensen, and M. A. Schmidt, "Micromachined Chemical Reactors for Surface Catalyzed Oxidation Reactions," Solid-State Sensor and Actuator Workshop, Hilton Head, SC, p. 15 (1996).
Wegeng, R. S., C. J. Call, and M. K. Drost, "Chemical Systems Miniaturization," Spring Meeting of the Amer. Inst. Chem. Eng., New Orleans, LA (1996).
Williams, W. R., M. T. Stenzel, X. Song, and L. D. Schmidt, "Bifurcation Behavior in Homogeneous-Heterogeneous Combustion: I. Experimental Results over Platinum," *Combust. Flame*, **84**, 277 (1991).
Wise, K. D., and K. Najafi, "Microfabrication Techniques for Integrated Sensors and Microsystems," *Science*, **254**, 1335 (1991).

Manuscript received May 7, 1997, and revision received Aug. 15, 1997.